This article has been accepted for publication in a future issue of this journal, but has not been fully edited. Content may change prior to final publication. Citation information: DOI 10.1109/JLT.2016.2606343, Journal of Lightwave Technology

Type-II $GaAs_{0.5}Sb_{0.5}$/InP Uni-Traveling Carrier Photodiodes with Sub-THz Bandwidth and High-Power Performance under Zero-Bias Operation

Jhih-Min Wun[1], Rui-Lin Chao[2], Yu-Wen Wang[1], Yi-Han Chen[1], and Jin-Wei Shi[1,3*], *Senior Member IEEE*

(Invited Paper)

***Abstract*—We successfully demonstrate ultra-fast uni-traveling carrier photodiodes (UTC-PDs) with sub-THz bandwidth (~170 GHz) and high-power performance under zero-bias and at 1.55 μm optical wavelength operation. By using a type-II ($GaAs_{0.5}Sb_{0.5}$/InP) absorption-collector interface and inserting an n-type (1×10^{18} cm^{-3}) charge layer in the collector, the current blocking (Kirk) effect can be greatly minimized. A stack of undoped $Al_xIn_{0.52}Ga_{0.48-x}As$ layers with different Aluminum mole fractions (x: 0.2 to 0.08) and bandgaps is adopted as the collector layer. This graded-bandgap design can provide a built-in electric field and further shorten the internal collector transit time. The demonstrated PD structure achieves a 3-dB optical-to-electrical bandwidth of 170 GHz and sub-THz output power -11.3 dBm at 170 GHz, a record among all the reported zero-bias PDs.**

***Index Terms*—photodiodes, high-power photodiodes**

I. INTRODUCTION

The amount of global network data traffic continues to grow, driven primarily by the use of wireless mobile data and internet video. The information and communication technology (ICT) sector is thus gradually coming to take up a larger portion of global electricity consumption (~10%) [1]. In order to minimize the demands of growth of the ICT sector, a large number of techniques have been adapted for energy-efficient processing of high-speed data streams in wireless [2] and wired networks [3,4]. Optical interconnect (OI) techniques [3,4], which could allow the replacement of the bulky and power-hungry active/passive microwave components with more energy-saving and high-speed optoelectronic devices, provide an revolutionary way to further reduce the carbon footprint of data centers and the wired network inside. However, the dc component of the high-speed optical data signal at the receiving end of an OI system still produces wasted heat energy, which is proportional to the product of dc reverse bias of the photodiodes (PDs) and the output photocurrent [5]. This heating effect could be a serious issue for the next generation of OI systems, which have densely packaged integrated circuits (ICs) with millions of optoelectronic components and optical channels forhigh-speed linking (>50 Gbit/sec) [6]. To have PDs that can sustain high-speed performance even under zero-bias operation would be an effective solutions to minimize this thermal issue. In addition, in an advanced coherent receiver array, which is used for the detection of optical signals with a complex modulation format for long-haul transmission, integration with a bulky broadband dc bias network with low electrical cross-talk (less than -30 dB) performance is necessary to handle the increased data rate capacity (> 100 Gbit/sec) [7]. However, the large geometric size of this bias network and its cross-talk performance will become an issue in a dense package of high-speed (> 100 Gbit/sec) coherent photo-receiver array with a compact size [7]. Clearly, a high-speed PD, which can be operated under the zero-bias condition is highly desired to minimize the footprint of its external bias circuit and electrical cross-talk.

The development of uni-traveling carrier photodiodes (UTC-PDs) [7-9], which have only fast electrons as speed-limiting carriers under a small external applied electric field (~ 10 kV/cm), would be one of the most attractive choices to satisfy the above-mentioned applications under zero-bias operation. This type of device structure has demonstrated an excellent 3-dB O-E bandwidth (>110 GHz) under a 1.2 mA output photocurrent [7] with a moderate saturation output power (-18.6 dBm at 2mA) at 100 GHz. Through the use of such a zero-bias PD integrated with a high-gain millimeter-wave (MMW) power amplifier, a low energy consumption photonic emitter module operated at around 100 GHz central frequency has been successfully demonstrated for 11 Gbit/sec line-of-sight wireless transmission [10]. In addition, in our previous work, with a UTC-PD with a type-II absorption-collector interface ($GaAs/In_{0.5}Ga_{0.5}P$) [11], we further pushed the operation voltage to a forward bias (photovoltaic mode) to serve as a high-speed laser power converter for simultaneous dc electrical power generation and high-speed (10 Gbit/sec) data detection [11-13].

In this work, we demonstrate a novel UTC-PD design, where the speed performance is further enhanced to the sub-THz regime under zero-bias operation. By using a type-II ($GaAs_{0.5}Sb_{0.5}$/InP) absorption/collector interface [14] and $Al_xIn_yGa_{1-x-y}As$ graded bandgap structure in the collector layer, the current blocking (Kirk) effect can be minimized [11-13]. The device successfully demonstrated state-of-the-art high-speed performance (170 GHz 3-dB O-E bandwidth at 2mA output photocurrent) and output power (-11.3 dBm at 8 mA) at

Jhih-Min Wun[1], Yu-Wen Wang[1], and Yi-Han Chen[1] are with the [1]Department of Electrical Engineering, National Central University (NCU), Taoyuan, 320, Taiwan. Rui-Lin Chao[2] is with the Department of Photonics, National Chiao-Tung University, Hsinchu 300, Taiwan. Jin-Wei Shi[1,3*] is on leave from NCU and serves as a visiting professor at [3]Department of Electrical and Computer Engineering, University of California Santa Barbara (UCSB), CA, 93106. (*email: jwshi@ee.ncu.edu.tw[1], jwshi@ece.ucsb.edu[3]).

This article has been accepted for publication in a future issue of this journal, but has not been fully edited. Content may change prior to final publication. Citation information: DOI 10.1109/JLT.2016.2606343, Journal of Lightwave Technology

the sub-THz regime (170 GHz) under zero-bias and 1.55 μm optical wavelength operation. Compared with our previous work [15], there is significant improvement in the bandwidth and saturation power due to the reduction in the differential resistance of the fabricated devices. To the best of our knowledge, this is the highest CW output power ever reported for photonic generation of sub-THz waves from a PD under zero-bias operation [7-9].

II. Device Structure and Design

Figure 1 shows the simulated band diagram for the demonstrated device structure under zero-bias operation. The position of the Fermi level is also specified; see the dotted line in the figure. The simulation was conducted using commercial software (ISE TCAD)[1]. Here, we adopted the $GaAs_{0.5}Sb_{0.5}$/InP type II absorption-collector (A-C) layer interface [14]. The p-type $GaSb_{0.5}As_{0.5}$ absorption layer with a thickness of 160 nm and a linearly graded doping profile (top: 5×10^{19} cm^{-3} to bottom: 1×10^{17} cm^{-3}) accelerates the electron diffusion process. This type of band alignment can provide injected electrons from the p-type $GaAs_{0.5}Sb_{0.5}$ layer to the InP collector layer with high excess energy (~0.22 eV) and minimize the current blocking effect, which is the major bandwidth limiting factor of UTC-PDs with type I A-C ($In_{0.53}Ga_{0.47}As$/InP) junctions under zero-bias operation [11,13]. In our collector layer, we adopted intrinsic InP and $In_{0.52}Al_xGa_{0.48-x}As$ layers with an ultra-low background doping density in order to relax the increase in junction capacitance and RC-limited bandwidth under zero-bias (nearly forward bias) operation [7,11]. However, the position of the simulated Fermi level suggests that in the proposed device structure, the undoped layers should become n-type doped layers under zero-bias due to the type-II band alignment in the A-C junction, as discussed above. This would lead to an increase in the junction capacitance and let the net optical-to-electrical (O-E) frequency responses be RC-limited. This issue will be discussed in detail later using the device modeling technique. The insertion of a thin (10 nm) n-type charge layer among these intrinsic layers at around the type II A-C junction results in a drop in the electron potential and further suppresses the current blocking effect [16]. In addition, a graded bandgap layer (GBL), comprised of three $In_{0.52}Al_xGa_{0.48-x}As$ layers with different mole fractions (x: 0.2 (top) to 0.08 (bottom)), is used as the collector layer to create a built-in electric field and accelerate the electron drift process. Among our GBLs, the longest cut-off wavelength for the $In_{0.52}Al_xGa_{0.48-x}As$ alloy ($In_{0.52}Al_{0.08}Ga_{0.4}As$), 1.46 μm (0.85 eV), is chosen in order to avoid any undesired absorption process under 1.55 μm wavelength excitation.

Figure 2 shows the simulated electric (E-) field distribution inside the absorption and collector layers for our device under zero-bias operation. The blue and red lines in this figure represent operation of the device under the dark condition and with an output photocurrent of 5 mA, respectively. The electron induced space-charge field inside this device is calculated assuming a reasonable electron drift-velocity (4×10^7 cm/sec) inside the collector layer and a 6 μm active diameter, which is the actual size of the fabricated PD.

[1]Synopsys, Inc., 700 East Middle field Rd., Mountain View, CA, 94043-4033, U.S.A.

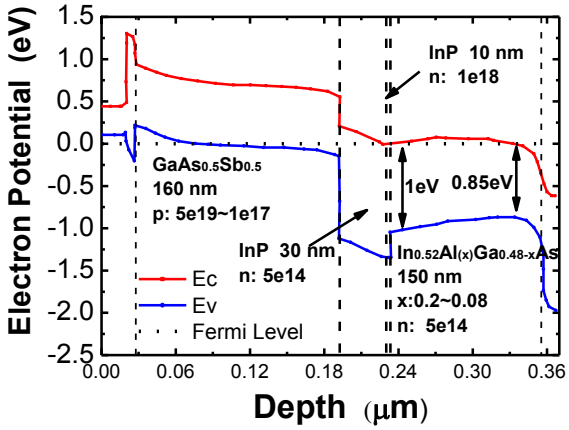

Figure 1. Simulated band diagram of demonstrated UTC-PDs under zero-bias operation. The unit of doping density is cm^{-3}.

In addition, for the 5 mA output photocurrent case, there is a shift in the effective bias voltage applied in the device simulation from zero to +0.25 V due to the fact that a load of 50 Ω is used during real measurement. Details of the calculation of the E-field inside the collector layers of the UTC-PDs can be referred to in our previous work [16]. As shown in Figure 2, the proposed GBL structure can produce a built-in electric field, which would not be screened by the high output photocurrent under zero-bias operation. As can be seen, under 5 mA output photocurrent, the net E-field in the A-C junction is nearly zero, which implies that a saturation phenomenon happens at this output current. This value is very close to the measured saturation current for our device, which will be discussed in detail later. Overall, the type II band alignment and graded bandgap layer in our proposed device structure induce a more significant built-in electron potential drop from anode to cathode than with the traditional UTC-PD. This is of great benefit to the speed and output power performance of the UTC-PD when there is no external applied bias voltage (electric-field).

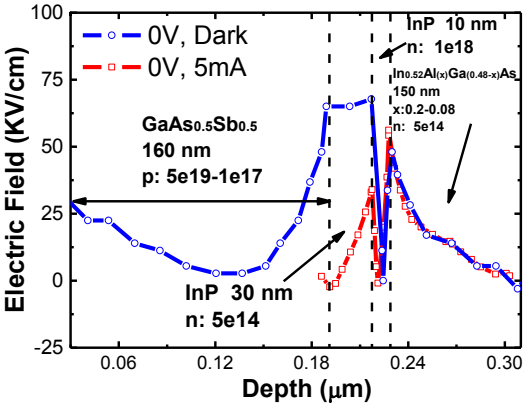

Figure 2. The simulated electric (E-) field distributions inside the absorption and collector layers of our demonstrated device structure under zero-bias operations. Blue line: E-field distribution without light illumination (dark). Red line: E-field distribution with 5 mA output photocurrent and under a 50 Ω load.

Figure 3 shows top-views of the active PD chip, co-planar waveguide (CPW) pad on the AlN substrate (for flip-chip bonding, which can provide nearly ~400 GHz 3-dB bandwidth [16]), and the PD chip after flip-chip bonding. The inset to

This article has been accepted for publication in a future issue of this journal, but has not been fully edited. Content may change prior to final publication. Citation information: DOI 10.1109/JLT.2016.2606343, Journal of Lightwave Technology

Figure 3 (a) shows an enlarged image of the fabricated PD which has a diameter of 6 μm and measured DC responsivity at ~0.09 A/W.

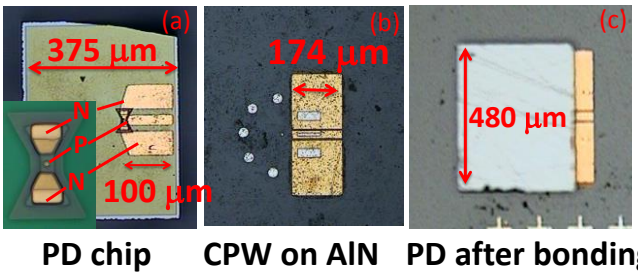

Figure 3. (a) Top-views of the active PD chip, (b) bonding pads on the AlN substrate, and (c) PD chip after flip-chip bonding. The inset in (a) shows a zoom in picture of the active PD.

III. Measurement Results and Discussion

A heterodyne beating system is used to measure the dynamic performance of the fabricated device structure. A power meter with a diode based sensor head, which covers the dc to 50 GHz frequency range is used for measurement. When the measurement frequency is greater than 75 GHz, a thermal MMW power meter (PM4, VDI-Erickson) is used. All the dynamic measurement results presented here, which include the O-E frequency responses and THz output power, have been carefully de-embedded to remove any contributions due to losses from the passive components used. From dc to 50 GHz, the frequency dependent loss of the passive components mainly originates from the radio-frequency (RF) coaxial cable and bias tee, typically around 8 dB at 50 GHz operation. The value of the frequency dependent loss was carefully verified using a broadband network analyzer (0.01 to 67 GHz). When the measurement frequency further increases (75-170 GHz), there are three major sources of insertion loss in our setup. The first is the frequency dependent insertion loss of the waveguide probe. For the WR-6 waveguide probe, which has a built-in bias tee, the loss is around 3 dB at 170 GHz operation, according to information provided by the manufacturer of the waveguide probe[2]. The second is the loss associated with the straight WR-10 waveguide section (0.185 dB at 170 GHz)[3], which is connected with the power sensor head. The last is from the waveguide taper (0.33 dB at 170 GHz)[3]. This component connects the WR-10 waveguide and the head of the waveguide probes (WR-6). After the calibration procedure, the corrected measured power values matched well at the edged frequency of the different bands, which included 50, 75, 110, and 170 GHz. This reveals the accuracy of the calibration procedures. Figures 4 to 6 show the measured bias dependent O-E frequency responses of the device from low (2 mA) to high (5 mA) output photocurrents, respectively. In each figure, the values of the data points in each O-E trace have been normalized to the output power of the PD at near dc (~1 GHz) and under zero-bias operation. The black trace in Figure 4 represents the extracted RC-limited frequency response of our demonstrated device, which will be discussed in detail later. We can clearly see that even under zero-bias operation with a moderate value of output photocurrent (2 mA), an extremely wide 3-dB O-E bandwidth (170 GHz) can be achieved. To the best of our knowledge, this is the best high-speed performance reported for any zero-bias photodiode [7-9]. Furthermore, the corresponding output photocurrent (> 2 mA) for the wide O-E bandwidth is high enough for most high-speed (100 Gbit/sec) photo-receiver circuit applications [6]. In addition, we can clearly see that under a low output photocurrent (2 mA), the measured bandwidth is insensitive to the reverse bias voltage (0 to -1 V). This implies that the built-in electric-field inside the active layers is strong enough to overcome the output photocurrent (~2 mA) induced space-charge-screening (SCS) effect. On the other hand, when the photocurrent reaches 5 mA, a saturation phenomenon is observed under zero-bias operation. Compared to the device under a -1 V bias, there is a ~2 dB drop in the output power in the zero-bias traces from near dc (~1 GHz) to the 3-dB bandwidth for the PD. This indicates that a higher reverse bias voltage (-1 V) is necessary to compensate for the SCS effect and minimize the degradation in speed performance for such a high output photocurrent (5 mA).

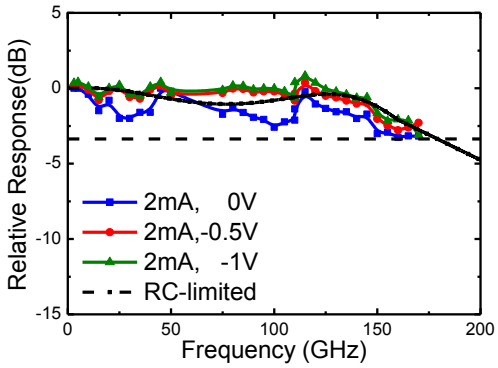

Figure 4. The measured bias dependent (0, -0.5, and -1V) O-E frequency responses with a 6 μm active diameter PD measured at an output photocurrent of 2 mA.

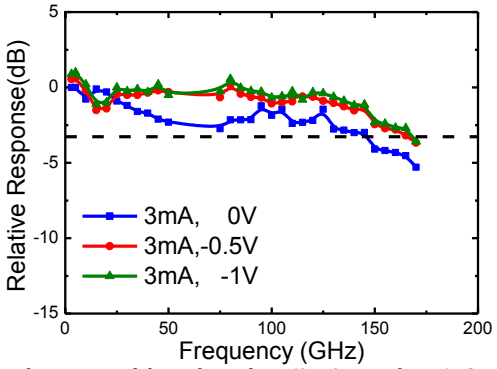

Figure 5. The measured bias dependent (0, -0.5, and -1V) O-E frequency responses with a 6 μm active diameter PD measured at an output photocurrent of 3 mA.

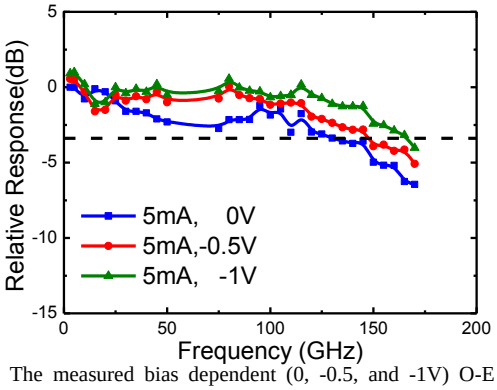

Figure 6. The measured bias dependent (0, -0.5, and -1V) O-E frequency responses with a 6 μm active diameter PD measured at an output photocurrent of 5 mA.

[2]Model 170; product of GGB Industries, Inc., P.O. BOX 10958, NAPLES, FL 34101

[3]Virginia Diodes, Inc., 979 Second Street, S.E. Suite 309, Charlottesville, VA 22902-6172. VDI APPLICATION NOTE: Power Measurement above 110 GHz

This article has been accepted for publication in a future issue of this journal, but has not been fully edited. Content may change prior to final publication. Citation information: DOI 10.1109/JLT.2016.2606343, Journal of Lightwave Technology

The net O-E 3-dB bandwidth (f_{3dB}) of a PD is determined by the carrier transit time ($1/f_t$) and the RC time constant ($1/f_{RC}$). We used the equivalent-circuit-modeling technique to investigate whether the internal carrier transit or RC-limited bandwidth dominates the measured net O-E bandwidth of our device [16-18]. With such an approach, the RC-limited bandwidth (f_{RC}) can be extracted by the use of the measured scattering parameters of the microwave reflection coefficients (S_{11}) [16-18] of the PD. Figure 7 (a) shows the adopted equivalent circuit models for the fitting of the S_{11} parameters and the fitted values of each circuit element, except for R_T and C_T, which are shown in the Table inserted into Figure 7 (b). Here, C_J, R_J, and R_C represent the junction capacitance, junction resistance, and differential resistance of the active p-n diode, respectively; C_P represents the parasitic capacitance induced by the interconnected metal lines between the passive CPW and active diode; R_P and L_P indicate the ohmic loss and inductance of the metallic CPW pads, respectively; and R_g and C_g represent the dielectric loss and capacitance caused by the buried dielectric layer (PMGI: Polymethylglutarimide) below the metal pads, respectively.

During the device modeling process for the extraction of the extrinsic f_{RC} for the PD chips, two artificial circuit elements (R_T and C_T) are removed, due to the fact that they are used to mimic the low-pass frequency response of the internal carrier transit time [16-18]. Figure 7 (b) shows the fitted and measured S_{11} parameters as a Smith Chart, while the extracted RC-limited frequency responses are given in Figure 4, as discussed above. We can clearly see that the fitted S_{11} trace matches the measured ones well, from nearly dc to 65 GHz (on the Smith Chart), and that the resonant frequency (~120 GHz) of the extracted RC-limited frequency response is very close to the net measured O-E one. These results are indicative of the accuracy of the proposed equivalent-circuit model. From the extracted RC-limited 3-dB bandwidth at around 175 GHz, we can conclude that the measured net O-E bandwidth (~170 GHz) is mainly determined by the RC time constant. The root cause of our large RC time constant might be the additional junction capacitance (C_j) induced by the non-depleted carriers, which originates from the type-II band alignment, as discussed in Figure 1. One feasible way to further relax the RC bandwidth and improve the net speed performance of the demonstrated device is to appropriately thicken the intrinsic layer. In addition, directly downscaling the device active area can also enhance the RC-bandwidth of the device, however, such an approach will usually lead to an increase in the differential resistance and significantly degradation in the speed performance of the PD under zero-bias operation [11,13]. In a previous work, we successfully demonstrated the use of an under-cut (mushroom) mesa structure to eliminate the trade-off between the junction capacitance and differential resistance in type-II GaAs/$In_{0.5}Ga_{0.5}P$ high-speed UTC-PDs for zero (forward) bias operation [13]. It might be possible to adopt this under-cut mesa structure to further improve the dynamic performance of this newly proposed type-II $Ga_{0.5}As_{0.5}Sb$/InP UTC-PD. Figures 8 and 9 show the transfer curves of the reverse bias voltages versus output photocurrent and normalized sub-THz power at 170 GHz, respectively. Here, two types of devices are measured for comparison. One is the proposed PD structure described in this paper and the other is the traditional $In_{0.53}Ga_{0.47}As$/InP UTC-PD structure with an additional n-type charge layer near the A-C interface [16]. Both devices share the same flip-chip bonding packaged structure and absorption/collector (~160/~160 nm) layer thicknesses.

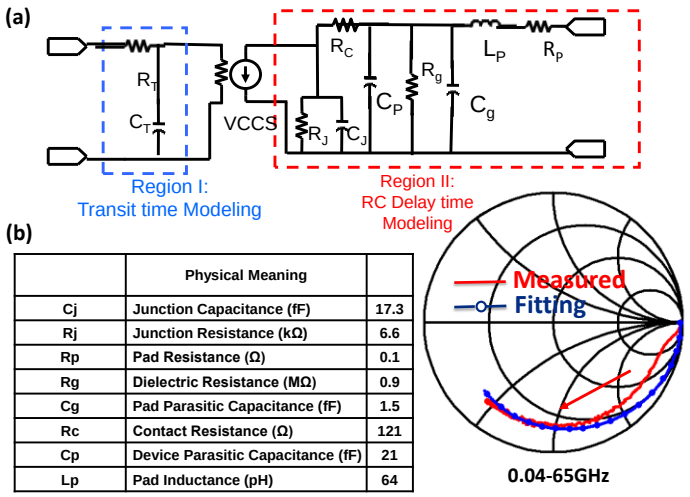

	Physical Meaning	
Cj	Junction Capacitance (fF)	17.3
Rj	Junction Resistance (kΩ)	6.6
Rp	Pad Resistance (Ω)	0.1
Rg	Dielectric Resistance (MΩ)	0.9
Cg	Pad Parasitic Capacitance (fF)	1.5
Rc	Contact Resistance (Ω)	121
Cp	Device Parasitic Capacitance (fF)	21
Lp	Pad Inductance (pH)	64

Figure 7. (a) Equivalent-circuit-model. VCCS: voltage controlled current source. (b) Measured (continuous line) and fitted (open circles) S_{11} parameters from near dc to 65 GHz under a fixed dc bias (0 V). The head of the red arrow indicates the increase in the sweep frequency. The inserted table shows the values of the circuit elements used in the modeling process.

We can clearly see that compared with the traditional UTC-PD, our proposed device structure shows a much smaller variation in both the photocurrent (0.7 vs. 2 mA) and sub-THz output power (2.8 vs. 26.1 dB) when the bias voltage swings from reverse to nearly forward (zero-bias). The measurement results strongly indicate the superior speed and power performance of our device compared to the traditional UTC-PD, under zero-bias operation.

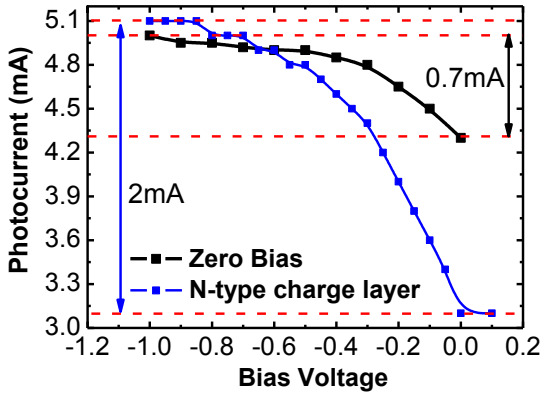

Figure 8. The measured transfer curve (bias voltage vs. photocurrent) at 170 GHz for the demonstrated type-II UTC-PD structure and reference UTC-PD structure.

This article has been accepted for publication in a future issue of this journal, but has not been fully edited. Content may change prior to final publication. Citation information: DOI 10.1109/JLT.2016.2606343, Journal of Lightwave Technology

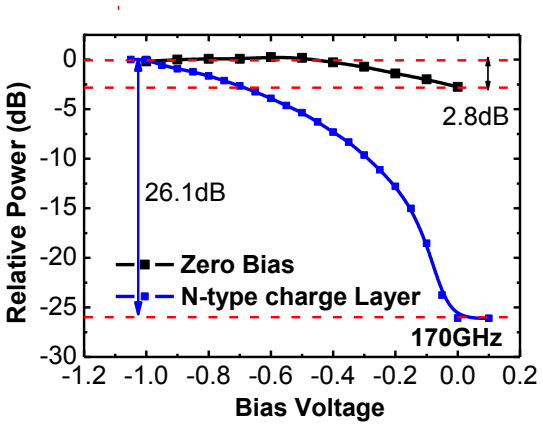

Figure 9. The measured transfer curve (bias voltage vs. output MMW power) at 170 GHz for the demonstrated type-II UTC-PD structure and reference UTC-PD structure.

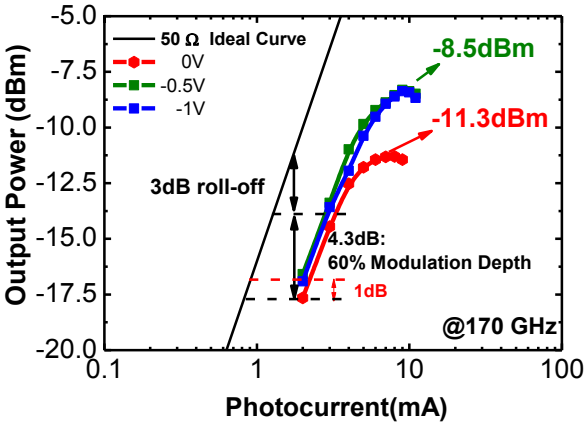

Figure 10. The measured photo-generated MMW power versus photocurrent under sinusoidal signal excitation and different reverse bias voltages (0, -0.5, and -1 V) at an operating frequency of 170 GHz. The solid line shows the ideal trace for a 100% modulation depth and 50 Ω load.

Figure 10 shows the photo-generated MMW power versus output photocurrent obtained with our PD under sinusoidal signal excitation at the 170 GHz operating frequency. The output power was measured by a thermal THz power meter (PM4, VDI-Erickson) and the value of the THz power shown here has been carefully de-embedded, taking into account an insertion loss of around 3 dB for D-band WR-6 waveguide probe, 0.33 dB for the waveguide taper (WR-6 to WR-10), and 0.185 dB for WR-10 waveguide section at the 170 GHz operation frequency. As can be seen, the optimum bias for maximum output power should be around -0.5 V and there is around a 3 dB enhancement in saturation output power compared to that obtained under zero-bias operation. This result differs from our O-E frequency response measurement results, which were illustrated in Figures 4 to 6, suggesting that the optimum bias for high-speed performance under high output photocurrent is -1 V. The drift in the optimum bias can be attributed to the differences between the two devices, with different values of differential resistances of ~70 and ~100 Ω, used for power and speed measurement, respectively.

We can clearly see that under zero-bias operation, there is significant saturation in the output power when the photocurrent is over 5 mA, which is consistent with our calculation results, as illustrated in Figure 2. Furthermore, compared with the results reported for the traditional UTC-PD with the $In_{0.53}Ga_{0.47}As$/InP A-C junctions and excellent performance in terms of speed and power under zero-bias operation [7], our device have an ~7.3 dB higher output power (-11.3 vs. -18.6 dBm), a higher saturation current (8 vs. 2 mA), and at a higher operation frequency (170 vs. 100 GHz). To the best of our knowledge, this is the highest CW output power ever reported for photonic generation of sub-THz waves from a PD under zero-bias (bias-free) operation [7-9]. Besides, as specified in this figure, there is an approximately 7.3 dB difference in power between the ideal (100% optical modulation depth) and measured traces. Such a discrepancy can be attributed to that the 3-dB high-frequency roll-off of the device itself at 170 GHz operation and the around 60% optical modulation depth in our optical system during power measurement, which corresponds to the other 4.3 dB loss of power.

IV. Conclusion

In this study we demonstrate a novel UTC-PD structure with state-of-the-art high-power and high-speed performance under zero-bias operation. Through the use of a type-II A-C junction and graded bandgap collector, the device, with an advanced flip-chip bonding package, exhibits an extremely wide O-E bandwidth (170 GHz), reasonable responsivity (0.09 A/W), and a moderate value of output power (-11.3 dBm) at the sub-THz regime (170 GHz) under zero-bias operation. The proposed device structure may find applications in next-generation OI or coherent fiber communication systems, where the densely packaged high-speed (100 Gbit/sec) photo-receiver array with extremely small thermal/electrical cross-talks and compact module size is highly desired.

V. Acknowledgement

This project is sponsored by the Ministry of Science and Technology of Taiwan under grant number MOST 102-2221-E-008 -092 -MY3.

References

[1] G. Cook, D. Pomerantz, K. Rohrbach, B. Johnson, and J. Smyth, *Clicking Clean: A Guide to Building the Green Internet.* Washington, D.C.: Greenpeace Inc., 2015, ch. 1.

[2] B. Kellogg, V. Talla, S. Gollakota, and J. R. Smith, "Passive Wi-Fi: Bringing Low Power to Wi-Fi Transmissions," *Proc. NSDI'16, Santa Clara*, CA, USA, March, 2016, pp. 151-164.

[3] P. Moser, P. Wolf, G. Larisch, H. Li, J. A. Lott, and D. Bimberg, "Energy-efficient oxide-confined high-speed VCSELs for optical interconnects," *Proc. SPIE, Vertical-Cavity Surface Emitting Lasers XVIII*, vol. 9001, pp. 900103, Feb., 2014.

[4] M. A. Taubenblatt, "Optical Interconnects for High-Performance Computing," *IEEE/OSA Journal of Lightwave Technology,* vol. 30, No. 4, pp. 448-458, Feb., 2012.

[5] H. Chen A. Beling, H. Pan, and J. C. Campbell, "A Method to Estimate the Junction Temperature of Photodetectors Operating at High Photocurrent," *IEEE J. Quantum Electron,* vol. 45, pp. 1537-1541, Dec., 2009.

[6] D. M. Kuchta, A. V. Rylyakov, C. L. Schow, J. E. Proesel, C. W. Baks, P. Westbergh, J.S. Gustavsson, and A. Larsson, "A 50 Gb/s NRZ Modulated 850 nm VCSEL Transmitter Operating Error Free to 90 ˚C," *IEEE/OSA Journal of Lightwave Technology,* vol. 33, no. 4, pp. 802-810, Feb., 2015.

[7] T. Umezawa, K. Akahane, N. Yamamoto, A. Kanno, K. Inagaki, and T. Kawanishi "Zero-Bias Operational Ultra-Broadband UTC-PD above 110 GHz for High Symbol Rate PD-Array in High-Density Photonic Integration," *OFC 2015, Los Angeles,* CA, USA, March, 2015, pp. M3C.7.

[8] H. Ito, S. Kodama, Y. Muramoto, T. Furuta, T. Nagatsuma, T. Ishibashi, "High-Speed and High-Output InP-InGaAs Unitraveling-Carrier Photodiodes," *IEEE J. of Sel. Topics in Quantum Electronics,* vol. 10, pp.709-727, Jul./Aug., 2004.

[9] T. Ishibashi, Y. Muramoto, T. Yoshimatsu, and H. Ito, "Unitraveling-Carrier Photodiodes for Terahertz Applications," *IEEE J. of Sel. Topics in Quantum Electronics,* vol. 20, pp. 3804210, Nov./Dec., 2014.

[10] T. Umezawa, K. Kashima, A. Kanno, K. Akahane, A. Matsumoto, N. Yamamoto, and T. Kawanishi, "11-Gbps 16-QAM OFDM Radio over Fiber Demonstration using 100 GHz High-Efficiency Photoreceiver based on Photonic Power Supply," *Proc. OECC/PS 2016, Niigata*, Japan, July, 2016, ThD3-3.

[11] Jin-Wei Shi, Cheng-Yo Tsai, Chan-Shan Yang, Feng-Ming Kuo, Yue-Ming Hsin, J. E. Bowers, and Ci-Ling Pan, "GaAs/$In_{0.5}Ga_{0.5}P$ Laser Power Converter with Undercut Mesa for Simultaneous High-Speed Data Detection and dc Electrical Power Generation," *IEEE Electron Device Lett.,* vol. 33, pp. 561-563, April, 2012.

[12] Jhih-Min Wun, Jin-Wei Shi, Cheng-Yo Tsai, and Yue-Ming Hsin, "Undercut GaAs/$In_{0.5}Ga_{0.5}P$ High-Speed Laser Power Converter for Simultaneous 10 Gbit/sec Data Detection and Efficient dc Electrical Power Generation," *2012 International Conference on Solid State Devices and Materials,* Kyoto, Japan, A-6-5, 2012.

[13] J.-W. Shi, F.-M. Kuo, Chan-Shan Yang, S.-S. Lo, and Ci-Ling Pan, "Dynamic Analysis of Cascade Laser Power Converters for Simultaneous High-Speed Data Detection and Optical-to-Electrical dc Power Generation," *IEEE Trans. on Electron Device.* vol. 58, pp. 2049-2056, July, 2011.

[14] L. Zheng, X. Zhang, Y. Zeng, S. R. Tatavarti, S. P. Watkins, C. R. Bolognesi, S. Demiguel, and J. C. Campbell "Demonstration of High-Speed Staggered Lineup GaAsSb–InP Unitraveling Carrier Photodiodes" *IEEE Photon. Technol. Lett.,* vol. 17, pp. 651-653, March, 2005.

[15] Jhih-Min Wun, Yu-Lun Zeng, and Jin-Wei Shi, "$GaAs_{0.5}Sb_{0.5}$/InP UTC-PD with Graded-Bandgap Collector for Zero-Bias Operation at Sub-THz Regime," *Proc. OFC 2016, Anaheim*, CA, USA, March, 2016, pp. Tu2D.4.

[16] Jhih-Min Wun, Hao-Yun Liu, Yu-Lun Zeng , Shang-Da Yang, Ci-Ling Pan, Chen-Bin Huang, and Jin-Wei Shi, "Photonic High-Power CW THz-Wave Generation by Using Flip-Chip Packaged Uni-Traveling Carrier Photodiode and Femtosecond Optical Pulse Generator," *IEEE/OSA Journal of Lightwave Technology,* vol. 34, pp. 1387-1397, Feb., 2016.

[17] Jhih-Min Wun, Cheng-Hung Lai, Nan-Wei Chen, John E. Bowers, and Jin-Wei Shi "Flip-Chip Bonding Packaged THz Photodiode With Broadband High-Power Performance," *IEEE Photon. Technol. Lett.,* vol. 26, no. 24, pp. 2462-2464, Dec., 2014.

[18] J.-W. Shi, C.-Y. Wu, Y.-S. Wu, P.-H. Chiu, and C.-C. Hong, "High-Speed, High-Responsivity, and High-Power Performance of Near- Ballistic Uni-Traveling-Carrier Photodiode at 1.55μm Wavelength," *IEEE Photon. Technol. Lett.,* vol. 17, pp. 1929-1931, Sep., 2005.

.